JOURNAL OF PROPULSION AND POWER
Vol. 22, No. 2, March–April 2006

Low-Order Modeling of Low-Frequency Combustion Instabilities in Aeroengines

Johannes Eckstein* and Thomas Sattelmayer†
Technical University of Munich, 85747 Garching, Germany

Rumble is a combustion-induced instability occurring in aeroengines during start-up. Characteristically, low-limit-cycle frequencies between 50 and 150 Hz are obtained. Two basic feedback mechanisms are susceptible to promote rumble: entropy waves being reflected as pressure waves at the (nearly) choked combustor outlet and the purely thermoacoustic mode, originating from an in-phase oscillation of the heat release and the combustor pressure. Prior experiments on a generic rich-quench-lean (RQL) combustor have shown that the thermoacoustic mode determines the instability behavior over a wide range of operating conditions. A low-order model is developed for the staged RQL combustor to replicate theoretically the experimental findings and to investigate further the interaction of entropy waves and the purely thermoacoustic mode. The model accounts for dispersion and incorporates a simple flame transfer function, developed for spray combustion with negligible prevaporization. The model results confirm the experimental findings indicating a dominating thermoacoustic mode in the spectrum. The characteristically low-limit frequencies are a result of the characteristic timescales of droplet transport and combustion in the primary zone. It is further shown that the prevailing instability mode is strongly dependent on the dispersive properties of the primary zone and in the dilution sector of the combustor.

Nomenclature

A	=	area, m^2
c	=	speed of sound, m/s
c_p	=	isobaric heat capacity
d	=	diameter, m
d_{32}	=	Sauter mean diameter, m
f	=	frequency, Hz
M	=	Mach number
$\dot{m}$	=	mass flow, kg/s
N	=	droplet number density, m^{-3}
p	=	pressure, Pa
$\dot{Q}$	=	heat release, W
$\dot{q}$	=	specific heat release of a droplet, W
T	=	temperature, K
t	=	time, s
u	=	axial velocity, m/s
Z	=	acoustic impedance, kg/m^2s
γ	=	ratio of specific heats
$\Delta\tau/\tau$	=	dispersion rate
ζ	=	injector pressure loss coefficient
Θ	=	dispersion function
Ξ	=	growth rate
ξ	=	atomizer sensitivity factor
ρ	=	density, kg/m^3
σ	=	surface tension, N/m
τ	=	characteristic timescale, s
ϕ	=	equivalence ratio
ω	=	angular frequency, 1/s

Superscript

$'$	=	perturbation

Received 25 January 2005; revision received 4 July 2005; accepted for publication 18 July 2005.

*Research Scientist, Lehrstuhl für Thermodynamik; eckstein@td.mw.tum.de.

†Professor, Lehrstuhl für Thermodynamik; sattelmayer@td.mw.tum.de.

I. Introduction

THE requirement for NO_x abatement in technical combustion systems led to the development of low-emission combustion technologies, such as rich-quench-lean (RQL) and lean-premix-prevaporized combustion. However, the flames obtained still suffer from a weak dynamic stability, resulting in oscillations of the combustor pressure and the heat release. One particular instability is commonly referred to as rumble and is observed in liquid-fueled aeroengine combustors during start-up, exhibiting characteristically low-limit-cycle frequencies between 50 and 150 Hz.

Various mechanisms were found to excite self-sustained combustion instabilities. Their relative importance varies with the combustion technology applied. For rumble, which is predominantly observed for diffusion flames, the impact of entropy waves on instability was usually considered to prevail.[1] Pressure feedback is induced if entropy waves are convected through a choked combustor outlet.[2] The typical low-limit frequencies were interpreted as an indicator for the higher convection times of entropy waves in the combustor.[3] However, recent experiments on generic RQL systems have shown that a purely thermoacoustic instability at characteristically low frequencies can also be obtained without choked outlet conditions as long as pressure variations at the injector lead to a considerable modulation of droplet number sizes and densities.[4] The burner sensitivity to acoustic perturbations is known from previous experimental[5,6] and numerical investigations[2] to be a critical element in the feedback loop, because it essentially determines the properties of the fuel spray supplied to the flame. In addition, the dispersion induced by the highly turbulent combustor aerodynamics can significantly alter the relative importance of potential instability drivers.[7]

Low-order modeling is a useful and efficient method for assessing the linear stability of complex thermoacoustic systems and is often applied for parametric analysis aimed at improved combustor design.[8–10] However, detailed knowledge is required regarding the underlying mechanisms leading to instability, in particular the mechanisms of heat production by the flame. In the past, most of the modeling efforts were accomplished in context with premixed flames.[11] Only a few attempts were made to extend network analysis to diffusion flames, particularly due to the additional complexities induced by droplet dynamics and evaporation.[12–14] This paper extends the method of linear modeling to spray flames for the particular case of rumble, based on the mechanisms observed in previous measurements.[4,15,16]

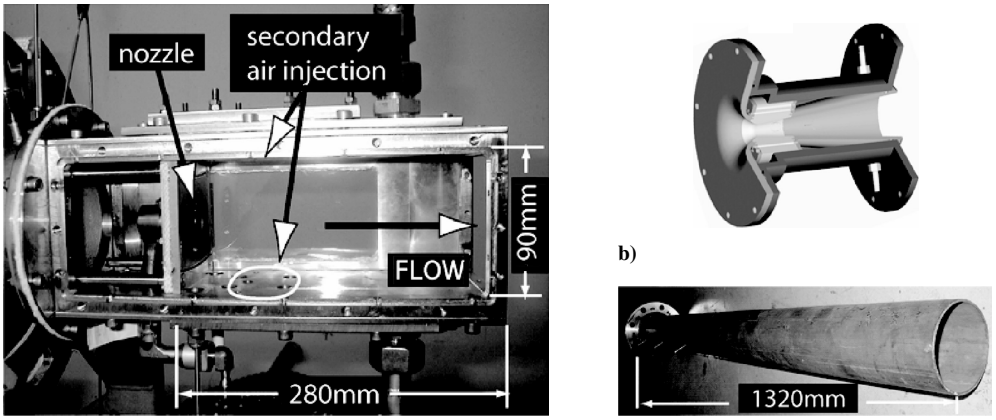

Fig. 1 Experimental setup: a) generic RQL combustor, with b) extensions choked venturi and c) $\lambda/4$ open-ended resonance tube.

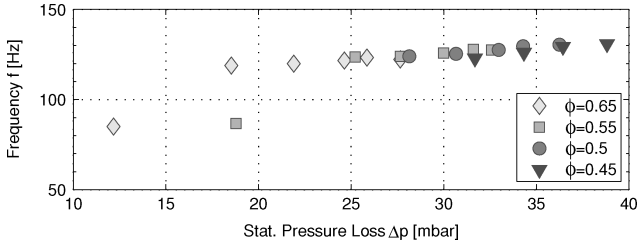

Fig. 2 Limit-cycle frequencies f of pressure oscillations in choked combustion chamber as a function of applied injector pressure loss Δp for variable equivalence ratios ϕ.

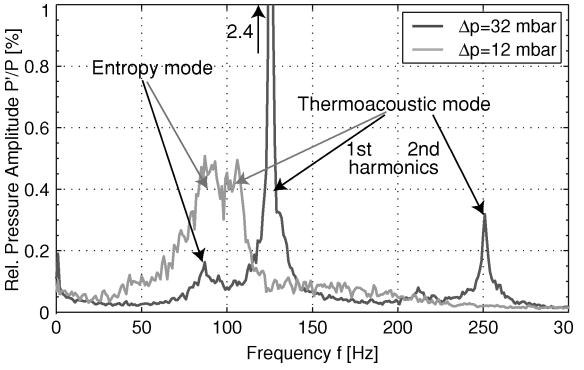

Fig. 3 Amplitude spectrum of pressure oscillations in limit cycle for variable pressure losses Δp.

II. Summary of Prior Experimental Results

The low-order model developed is based on experimental results,[4,15,16] which will be briefly summarized. The experiments were conducted using a generic single-sector RQL combustor incorporating a triple-swirl airblast atomizer, as shown in Fig. 1. The atomizer design is typical for aeroengines. The combustor dimensions and the hole pattern in the quenching zone for secondary injection were derived from the real annular liner geometry. Dilution, film, and liner cooling were omitted. Approximately 40% of the overall air mass flow enters the combustion chamber through the front panel and 60% as secondary admix air in the flame quenching zone. The supply section of the secondary air injection is acoustically decoupled from the combustor using perforated plates, and the overall quenching flow was controlled by a metering valve.

The combustion chamber was operated under near-ambient pressure conditions up to 1.6 bar static pressure (absolute) at constant air inlet temperature (300 K), thus closely corresponding to start-up conditions of aeroengines, where "rumble" predominantly occurs. A venturi nozzle was applied to the combustor outlet, imposing choked exit conditions. Alternatively, an open-ended flame tube was mounted to the combustor, imposing a comparably low outlet admittance to the (unextended) combustor, but without flow acceleration and reflection of entropy waves. The length of the tube was chosen to approximate a quarter-wavelength of the rumble oscillations observed in the combustor. The self-excited combustion-induced oscillations were measured in the limit cycle under varying air and fuel mass flows, using microphones (dynamic pressure), a double thermocouple probe (temperature fluctuations),[16,17] and OH^* chemiluminescence, which proved to be an adequate measure for the phase of the oscillating heat release.[4]

Figure 2 shows the dominating frequencies in the limit cycle obtained for the venturi for changing injector pressure loss Δp. Self-excited instability modes occurred with rumble-typical limit-cycle frequencies between 80 and 135 Hz. Two distinct frequency bands are observed in Fig. 2, which are associated with two different excitation modes. The excitation modes could be distinguished experimentally by temperature measurements in the combustor and by varying the combustor extension. The higher-frequency band, between 118 and 135 Hz, was shown to be associated with a purely thermoacoustic mode, and the instability could be reproduced using the open resonance tube extension of Fig. 1.[4] Choked outflow conditions and the reflection of entropy waves are thus not a prerequisite for this instability mode. In the lower-frequency band between 80 and 100 Hz, however, entropy waves drive the instability. A corresponding instability band was not observed in the pressure spectrum for the open resonance tube. With venturi, both instability modes coexist in the combustion chamber in the limit cycle, exhibiting variable relative strength as shown in Fig. 3. Because the characteristic wavelengths of the rumble mode lie in the range of several meters and exceed the length of the (unextended) combustor by a factor 20, the combustor pressure oscillates in the bulk mode. As a consequence, the dominating instability frequencies showed to be essentially determined by the characteristic timescale of droplet transport from the nozzle to the flame τ_d and by the entropy convection time τ_s in the dilution sector of the combustor, depending on the prevailing instability mode.

For most operating conditions, the dominant instability mode proved to be purely thermoacoustic, according to Fig. 3. The necessary condition for self-excitation proved to be a low combustor outlet admittance, as obtained for both the venturi and the flame tube. Under those conditions, significant pressure oscillations are obtained at the nozzle, which modulate the effective pressure drop and the droplet sizes obtained during atomization.[4] The droplet delay time τ_d essentially determines the coupling of dynamic pressure and heat release in the combustor and, thus, the growth rates of the oscillation. The measured time traces of pressure and heat release showed a typical phase lag between 45 and 65 deg, thus satisfying the Rayleigh criterion (see Ref. 16). For the operation at low injector pressure losses during engine start-up, even small fluctuations of the air

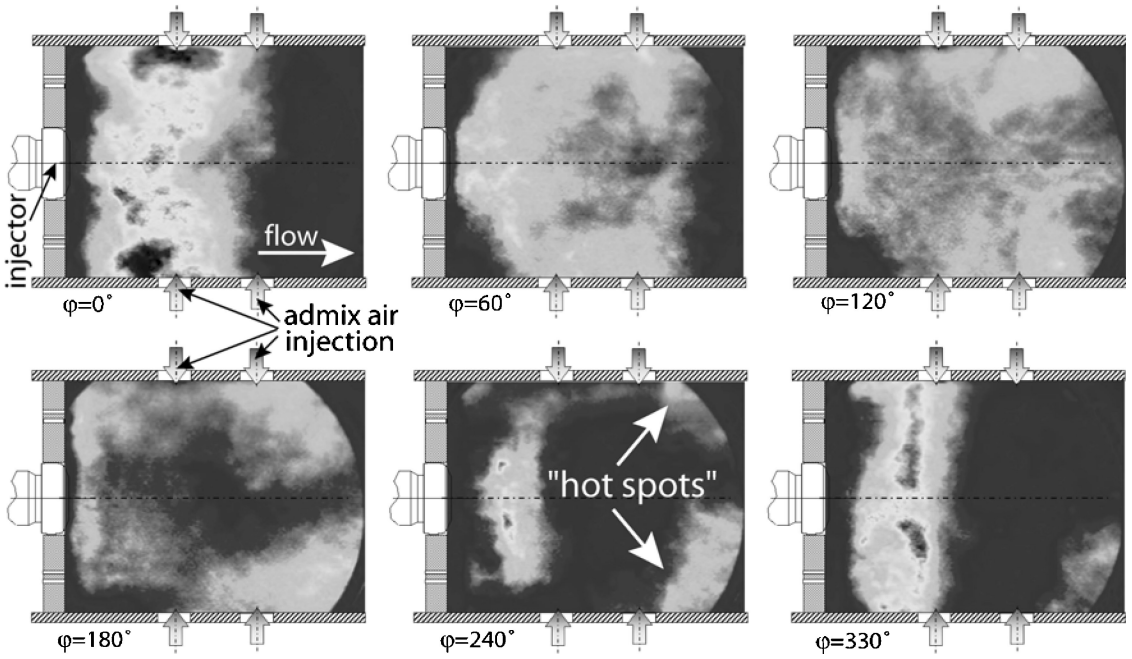

Fig. 4 Phase-resolved high-speed camera recording of flame OH* chemiluminescence during one oscillation cycle at 126 Hz ($\Delta p/p = 2.3\%$, $\phi = 0.55$, $T_{air} = 300$ K); flow direction left to right, front panel, including heatshield and injector, is on left-hand side; four opposits rows of admix injection indicated by gray arrows.

velocity remarkably alter the average droplet size and the droplet number density. Both parameters in turn strongly influence the combustion rates and heat release of the flame. For this reason, the occurrence of self-excited combustion instabilities is intrinsically tied to the atomizer sensitivity toward changing air mass flows. A highly dispersive flow in the primary zone, for example, for increased swirl, proved to increase the mixing of the droplets and to homogenize the diameter variations while traveling to the flame. This globally reduced the tendency for instability and the limit-cycle amplitudes obtained. The relatively low-limit-cycle frequencies of the (thermoacoustic) rumble mode are related to the low Mach number of the combustor flow and the extended timescales for transport, evaporation, and combustion of the generally larger fuel droplets. For the operating conditions investigated, $2.3 < \tau_d < 3.1$ ms could be deduced from the measured phase difference between dynamic pressure and heat release, with a tendency to rise with average droplet size.

A phase-resolved high-speed recording of the oscillatory heat release of the flame is shown in Fig. 4. Figure 4 also indicates the formation of hot spots or entropy waves. When the dynamic temperature is measured at variable axial locations in the combustor, it could be shown that the entropy waves travel with approximately bulk velocity toward the combustor outlet. Under the influence of the staged injection of admix air, nonuniform flow conditions and dispersion in the combustor are increased and entropy waves were found to be strongest close to the walls. Dispersion caused the amplitude of the entropy waves to diminish quickly, such that the effective strength at the nozzle inlet usually became too weak to alter significantly the dominating thermoacoustic mode of the primary zone.

When the injector pressure loss was lowered, the relative importance of the thermoacoustic mode decreased. Under conditions of low applied pressure loss, for example, $\Delta p = 12$ mbar in Figs. 3 and 5, the entropy mode started to dominate the overall instability behavior. This effect is linked with the larger droplet sizes produced and the correspondingly longer evaporation and burning timescales, leading to flames that extend into the dilution sector of the combustor. As a consequence, the generated entropy waves were less susceptible to dispersion in the quenching zone of the combustor. Nevertheless, their overall destabilizing effect was weak, inducing approximately 75% lower pressure amplitudes in the limit cycle than the thermoacoustic mode, as shown in Fig. 5.

Figure 5 shows the dynamic pressure amplitudes in the limit cycle as a function of the static pressure loss applied. Here $\Delta p'/p$ is

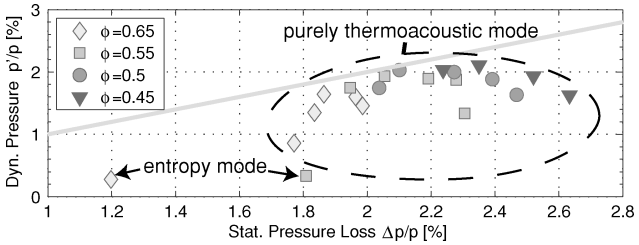

Fig. 5 Pressure amplitude $\Delta p'/p$ in limit cycle over normalized static pressure loss $\Delta p/p$.

the effective pressure loss across the burner, being modulated by the pulsating combustor pressure. The light gray line delimits the region where dynamic pressure oscillations would exceed the static pressure loss across the injector, leading to flow reversal through the burner and inhibiting the fuel transport to the flame. The static pressure loss characteristic of the injector is, hence, the upper limit for the attainable oscillation amplitudes of the thermoacoustic mode.

III. Low-Order Model

A low-order model was formulated for the RQL-configuration to replicate theoretically the experimental findings by a linear stability analysis of the system.[16] The linear network model describes the onset of instabilities by determining the unstable eigenfrequencies of the acoustic system. The experiments indicated that the key variables impacting the overall system stability are the acoustic pressure p' and velocity u', the droplet size fluctuations d' in the primary zone, and the entropy waves s' in the dilution sector.

For theoretical analysis, the overall system is decomposed into separate acoustic multiports, shown in Fig. 6, each representing a physical process in a specific sector of the combustor. The vector of variables of the network model, thus, contains 14 elements, $\boldsymbol{v} := \{p'_1, \ldots, p'_5, u'_1, \ldots, u'_5, d'_1, d'_3, s'_4, s'_5\}$, which are coupled by the 14×14 coefficient matrix $\boldsymbol{S}$, which describes the linear acoustic system. The system matrix $\boldsymbol{S}$ is in general complex and a function of the excitation frequency $f = \omega/2\pi$.

For eigenmode analysis, the homogeneous solution of the system of linear equations $\boldsymbol{S} \cdot \boldsymbol{v} \equiv 0$ is considered, which yields nontrivial solutions for $\det(\boldsymbol{S}) = 0$. The roots of this characteristic polynomial

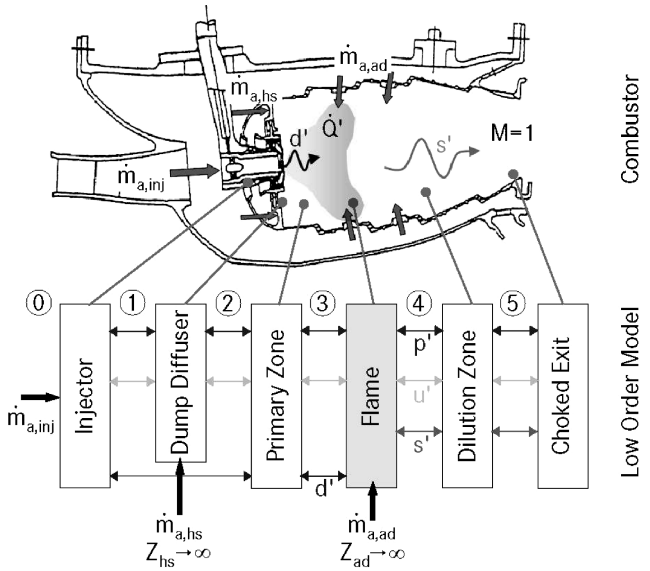

Fig. 6 RQL combustor[6] and low-order model.

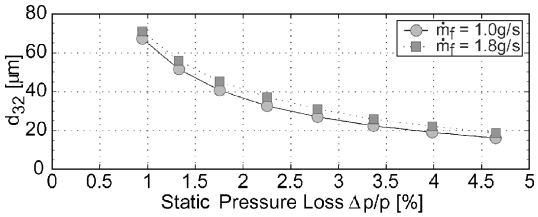

Fig. 7 Static injector reponse: Sauter mean diameter of the fuel spray as function of applied pressure loss, measured by Malvern particle sizing (see Ref. 15).

are the complex-valued eigenfrequencies $\hat{f}_e$. When a harmonic time dependence of the excitation $e^{i\omega t}$ is implied, the real part of the eigenfrequency $\mathrm{Re}(\hat{f}_e) = f_e$ determines the frequency of oscillation, whereas the imaginary part $\mathrm{Im}(\hat{f}_e)$ specifies the growth behavior of the corresponding eigenmode in time. The growth rate Ξ of an eigenmode is defined as the amplitude ratio of two successive oscillation cycles and can be calculated as

$$\Xi = \exp\{-2\pi[\mathrm{Im}(\hat{f}_e)/\mathrm{Re}(\hat{f}_e)]\} \tag{1}$$

Unstable eigenmodes are characterized by $\Xi > 0$. In the following subsections, the key elements of the acoustic system are presented for the limiting case of low instability frequencies. Novel elements are focused on, which are particular for the setup used. The remaining equations can be obtained from the given references. A detailed summary of all model equations may be found in Ref. 16.

A. Injector

The airblast injector is considered as a compact element that imposes acoustic boundary conditions on the system inlet. Furthermore, the atomizer characteristics determines the amplitude of the fuel droplet size fluctuations d_1' as response to acoustic velocity perturbations u_1' at the atomizer lip.

Prior measurements with the same injector have shown that both the pressure–velocity coupling and the spray–velocity coupling are quasi steady for excitation frequencies below 150 Hz (Ref. 15). The pressure–velocity coupling is then characterized by the Bernoulli equation for the linearized perturbations,

$$\tfrac{1}{2}(p_0' - p_1')/\Delta p = u_1'/u_1 \tag{2}$$

where the quantities without a prime denote the corresponding static values. Because the area change from the air supply section to the burner inlet is very large (for the test rig used, approximately 1:90) and no upstream forcing is applied, plenum conditions $p_0' \equiv 0$ can be assumed upstream of the injector. This assumption was experimentally proven by pressure measurements in the supply section, which showed negligible pressure oscillations even for heavy rumble in the combustor. Furthermore, the static pressure loss and the average air velocity in the burner are correlated by

$$2\Delta p = \rho_a(1+\zeta)u_1^2 \tag{3}$$

where ζ is the static pressure loss coefficient of the injector ducts, which is 6.4%, determined by pressure drop measurements. The average injection velocity of the air u_1 can be obtained by dividing the air volume flux with the burner area A_{inj}. When the preceding equations are combined, the coupling of the acoustic pressure and velocity at the injector outlet is finally derived as

$$u_1' = [-A_{\mathrm{inj}}/(1+\zeta)\cdot \dot{m}_{a,\mathrm{inj}}]p_1' \tag{4}$$

In the model, the polydisperse spray generated by the injector is assumed to be adequately represented by the Sauter mean diameter d_{32}. For low-viscosity fuels such as kerosene, the atomization process is governed by the Weber number We (see Ref. 18),

$$d/l \propto We^{-x} = (\rho u^2 d/\sigma)^{-x} \tag{5}$$

Equation (5) can be rewritten with respect to a reference state 0

$$d/d_0 = (u/u_0)^{-\xi}, \qquad \xi > 0 \tag{6}$$

The sensitivity of the generated droplet sizes to the injector air velocity is, thus, characterized by the exponent ξ. A rising ξ indicates stronger sensitivity. From the steady atomization characteristics for the injector shown in Fig. 7, a value of $\xi = 1.6$ was obtained. As already mentioned, further measurements have shown that the steady atomizer performance of Fig. 7 is still valid for low-frequency excitation.[15] Linearization of the quasi-steady diameter variations according to Eq. (6) yields

$$d_1'/d_1 = -\xi(u_1'/u_1) \tag{7}$$

Equations (4) and (7) are used to model the inlet boundary conditions imposed by the injector. The underlying assumption of a quasi-steady injector response was experimentally proven for the low-frequency domain below 150 Hz only, which restricts the applicability of the low-order model to that frequency range.

To model the coupling of the acoustic quantities u' and p' across the sudden area change between points 1 and 2 downstream of the injector exit, the transfer matrix of a compact dump diffuser with acoustic loss[19] is used. It is further assumed that the droplet sizes remain unchanged across this area change. The effects of flow recirculation and turbulence are considered in the dispersion function, which is derived in the following subsection.

B. Primary Zone Transport and Dispersion of Droplet Clusters

In the experiments, it was found that the dispersion induced by the aerodynamics in the combustor plays a determining role on the general instability behavior and must consequently be taken into account in the low-order model. The aerodynamics of the primary zone can increase the homogenization of the droplet clusters produced by the injector at different instants and will, therefore, favorably influence combustor stability.

A one-dimensional model for the aerodynamic dispersion of a fluctuating scalar Ψ' in a duct is proposed by Sattelmayer[7] based on a probability density function analysis of delay-time distributions under nonuniform flow conditions. The underlying idea is summarized in Fig. 8a: A perturbation pulse Ψ' of the scalar, applied uniformly over the inlet area of the duct, is subject to dispersion because the convective delay times, imposed by a nonuniform flow profile inside the duct, vary over the duct cross section. A smeared profile of the dispersed scalar is, therefore, obtained at the duct outlet after an average convection time τ. The dispersed profile of the scalar

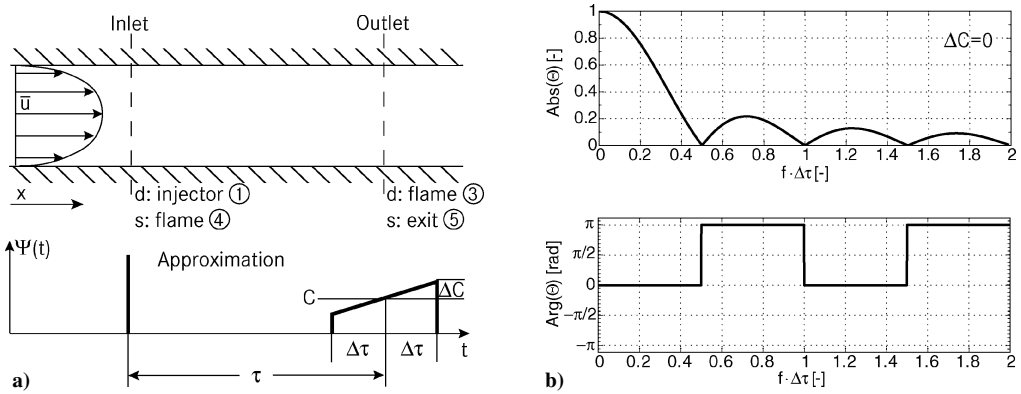

Fig. 8 Dispersion model: a) Schematic of dispersion acting on scalar pulse Ψ' in duct with nonuniform flow and b) dispersion function $\Theta(i\omega)$ for $\tau \equiv 0$, $\Delta C \equiv 0$ (Ref. 7).

can be idealized as trapezoid. For the simplifying case $\Delta C/C = 0$, the following coupling condition can be derived[7]:

$$\Theta(i\omega) = \frac{\Psi'_{\text{outlet}}}{\Psi'_{\text{inlet}}} = e^{-i\omega\tau} \cdot \frac{e^{i\omega\Delta\tau} - e^{-i\omega\Delta\tau}}{2i\omega\Delta\tau} = e^{-i\omega\tau} \cdot \frac{\sin(\omega\Delta\tau)}{\omega\Delta\tau} \quad (8)$$

$\Theta(i\omega)$ describes the influence of the dispersion on Ψ' as a function of the oscillation frequency ω. It is composed of a convective time lag (first term) and a integrator term (second term), which introduces a frequency-dependent damping of the scalar fluctuations. This dispersive term is plotted in Fig. 8b. The transfer characteristics of the duct is essentially given by the mean convection time τ and by the time spread $\Delta\tau$, which is a measure of the nonuniformity of the flow and the strength of the encountered dispersion. The ratio $\Delta\tau/\tau$ is, thus, a measure of the dispersion rate. It can be shown by series expansion that, for the limiting case $\Delta\tau \to 0$, the dispersion function $\Theta(i\omega)$ reduces to the simple convective time lag $e^{-i\omega\tau}$.

The amplitude of the average droplet size change d' produced at the atomizer lip over one oscillation period will be dampened on the way to the flame by the highly nonuniform flow in the primary zone, inducing a time spread $\Delta\tau_d$ for the droplet transport to the flame. This process can be understood as mixing and is purely related to the aerodynamics of the primary zone, independently of eventual droplet size changes occurring from secondary spray breakup or evaporation. Experiments with a similar injector[16] with higher swirl number have proven that the tendency for self-excitation is considerably decreased due to higher dispersion rates in the shear layers. With Eq. (8), the droplet size variability arriving at the flame front becomes

$$d'_3 = \Theta_d d'_1 \quad (9)$$

The convective time delay of the droplets τ_d entering Θ_d includes the subprocesses of droplet acceleration and convection. As already mentioned, it was estimated experimentally from the phase shift between heat release and pressure fluctuations. It ranges between $2.3 < \tau_d < 3.1$ ms, depending on the mean droplet size and the applied pressure loss.

The propagation of the acoustic quantities p' and u' in the primary combustor zone 2–3 is modeled one dimensionally, assuming a loss-free straight duct[7,20] at a fixed length of 40 mm, corresponding to the average flame standoff distance observed in the experiments.

C. Flame Transfer Function for Spray Flames in Low-Frequency Domain

In the case of premixed flames, velocity changes that alter the flame surface area are one important source of heat release fluctuations.[11] In the case of combusting sprays, no uniform equivalence ratio distribution in the flame can be presumed. The experimental results in Fig. 2 for the diffusion burner reveal a strong dependency on the injector pressure loss and, thus, on the droplet size. This suggests that, in the case of spray flames, the heat release fluctuations should be expressed as a function of the droplet size modulations (d'/d) that enter the reaction zone.

With respect to the low inlet temperatures of the air (300 K), the following assumptions are made to model the transfer function of the spray flame in the low-frequency domain.

1) The impedance of the fuel supply is assumed infinite, and the total fuel flow rate $\dot{m}_f$ is constant, due to the very compact fuel duct design of the injector and its low fuel storage capacity.

2) The impact of prevaporization is negligible, and the droplet diameters remain unaffected during the convection to the flame. Secondary spray breakup is neglected.

3) Because of staged air injection with high-turbulence levels, turbulent mixing and reaction are infinitely fast. Combustion is controlled by droplet evaporation. The evaporation process in the flame follows the D^2 law.[21] Each droplet burns in a spherical layer under stoichiometric conditions. The heat released by a single droplet is then proportional to the instantaneous fuel evaporation rate.

4) The length of the flame is very small compared to the occurring wavelengths ($\lambda > 4$ m), that is, the flame is compact.

5) Because the characteristic droplet burning times are usually small compared to the oscillation period $\tau_b \ll 1/f$, the heat release fluctuations are attributed exclusively to the droplet cluster arriving in the flame. As a further simplification, the time-dependent combustion rate of a burning droplet is replaced by the average heat release over the burning time.

Under the described conditions, the overall heat release of the flame $\dot{Q}$ becomes the product of the average heat released by a single droplet $\dot{q}$ and the droplet number density N. Both N and $\dot{q}$ are functions of the droplet diameter d. Linearization yields

$$\dot{Q}'/\dot{Q} = (N\dot{q})'/N\dot{q} = N'/N + \dot{q}'/\dot{q} \quad (10)$$

Under conditions of constant fuel mass flow, the droplet number density per unit volume is coupled with the droplet diameter by

$$\dot{m}_f = \frac{\mathrm{d}}{\mathrm{d}t}\left(N\frac{\pi}{6}\rho_f d^3\right) = \text{const} \quad (11)$$

Linearization yields the required function for the first term in Eq. (10),

$$(N'/N) = -3(d'/d) \quad (12)$$

With respect to the second term in Eq. (10), the instantaneous heat release of the fuel droplet $\dot{q}_d(t)$ is the product of the fuel evaporation rate of the spherical droplet $\dot{m}_d$ and the specific enthalpy of reaction h_b of the fuel,

$$\dot{q}_d(t) = \dot{m}_d h_b = -\frac{\pi}{6}\rho_f h_b \frac{\mathrm{d}}{\mathrm{d}t}[d(t)^3] = -\frac{\pi}{2}\rho_f h_b d^2 \frac{\mathrm{d}}{\mathrm{d}t}d(t) \quad (13)$$

Applying the D^2 law for the diameter change $d(t)$ of the burning droplet, the average heat release of a single droplet with initial

diameter d_0 finally becomes

$$\dot{q} = \frac{1}{\tau_b}\int_0^{\tau_b} \dot{q}_d(t)\,\mathrm{d}t = h_b \frac{\pi}{6}\rho_f K d_0 \tag{14}$$

K is the burning rate constant. The following linearized dependency is, thus, obtained for the average heat release fluctuations:

$$(\dot{q}'/\dot{q}) = (d'/d) \tag{15}$$

When Eqs. (12), (15), and (10) are combined, the following transfer function can be finally composed, adopting the indexing of Fig. 6:

$$(\dot{Q}'/\dot{Q}) = -2 \cdot (d_3'/d_3) \tag{16}$$

The expression Eq. (16) reflects the dominating effect of the droplet number density on the heat release, as observed in the experiments. The simplicity, particularly the independence from the frequency, is a result of neglecting finite burning times τ_b. Equation (16) is, therefore, only applicable in the low-frequency domain. A more common formulation of the flame transfer function, used in context with premix flame thermoacoustics, refers to relative velocity fluctuations (u'/u) (Ref. 11). In the case of the spray flame, an equivalent formulation could be obtained by backtracking the droplet path from the flame across the dispersive primary zone to the injector. Combining Eqs. (16), (9), and (7) yields

$$\dot{Q}'/\dot{Q} = 2\xi\Theta_d(u_1'/u_1) \tag{17}$$

The heat release fluctuations of the spray flame, thus, depend on the atomizer sensitivity, the velocity fluctuations at the atomizer lip, and the aerodynamics of the primary zone.

The coupling of the acoustic variables over the flame front is given by the Rankine–Hugoniot relations (see Refs. 22 and 23). With Eq. (16), one obtains, with $\dot{Q} = \dot{m}_f h_b$,

$$p_4' = p_3' \tag{18}$$

$$u_4' = u_3' - 2(\dot{m}_f h_b/A_{cc})\left[(\gamma-1)\Big/c_3^2\rho_3\right](d_3'/d_3) \tag{19}$$

With Eq. (16), the entropy wave s_4', generated by the flame, is calculated as

$$s_4' = c_p(1 - T_3/T_4)(\dot{Q}'/\dot{Q}) = -2c_p(1 - T_3/T_4)(d_3'/d_3) \tag{20}$$

D. Staged Air Injection

One particular feature of the investigated combustor is the staged injection of the air. As indicated in Fig. 6, the overall air mass flow is separately fed into the combustion chamber through the injector $\dot{m}_{a,\mathrm{inj}}$, the front panel heat shield $\dot{m}_{a,\mathrm{hs}}$ and the admix orifices in the quenching zone $\dot{m}_{a,\mathrm{ad}}$. The area ratio between the cooling holes in the heat shield and the combustion chamber is very high. Furthermore, the admix orifices were acoustically decoupled in the experimental setup using perforated plates, which induced considerable pressure loss. Infinitely high impedances Z were, therefore, assumed for the heatshield and the admix inlets, without any modulation of the entering air. The only acoustically active inlet, thus, remains the airblast atomizer according to Eq. (4).

Mass flows $\dot{m}_{a,\mathrm{hs}}$ and $\dot{m}_{a,\mathrm{ad}}$ impact the overall system by increasing the mean velocities downstream of the corresponding inlet. The effect of the staged injection of air is accounted for by applying the dissipation function Eq. (8) for the primary and the dilution zone. Because the highly turbulent combustor aerodynamics will tend to homogenize the average temperatures up- and downstream of the flame, the temperature distribution in the model combustor is simplified being split into two homogeneous temperature zones up- and downstream of the flame. The upstream temperatures $T_1, \ldots, T_3$ are approximated by the inlet air temperature, which was kept at 300 K during the experiments. The downstream temperature was set to the adiabatic value $T_4 = T_5 = T_{\mathrm{ad}}(\phi)$ for the applied overall equivalence ratio.

E. Dilution Sector of the Combustor Dispersion of Entropy Waves

As for the primary zone 2–3, the dilution zone 4–5 of the combustor is modeled as loss-free straight duct including one-dimensional propagation of the acoustic quantities p' and u'. The dispersion obtained in the dilution zone of the combustor affects the magnitude of the traveling entropy waves and the amplitude of the pressure wave reflected at the sonic nozzle. Equation (8) is also applied to describe the entropy dispersion,

$$s_5' = \Theta_s s_4' \tag{21}$$

Because the entropy wave are known to travel approximately with bulk velocity in the combustor, the average delay time τ_s can be obtained by

$$\tau_s = l_4/u_4 = l_4 A_{cc}/\dot{m}_a\rho_4 = V_4/\dot{m}_a\rho_4 \tag{22}$$

where V_4 is the volume of the dilution zone.

The choked and isentropic exit nozzle determines the acoustic boundary condition at the combustor exit. The interaction between p' and u' and the impinging entropy wave s' is given by[2]

$$u_5' = [(\gamma-1)/2]M_5(p_5'/\rho_5 c_5) + M_5(c_5/2)(s_5'/c_p) \tag{23}$$

IV. Results

In a first step, the thermoacoustic behavior of the combustor is discussed, neglecting the existence of the entropy waves in the dilution zone. This is accomplished by setting $s_4' \equiv 0$. The outlet admittance is low because $M_5 \ll 1$, according to Eq. (23). The results are, thus, comparable with the measurements that were obtained using the flame tube extension in Fig. 1.

In Fig. 9a, the growth rate Ξ according to Eq. (1) is plotted over the eigenfrequencies $f_e = \mathrm{Re}(\hat{f}_e)$ of the combustor. The droplet dispersion rate $\Delta\tau_d/\tau_d$ is used as parameter. The bold black line at $\Xi = 1$ separates the instability region, $\Xi > 1$, from the stable modes, $\Xi < 1$. The vertical lines in the graphs show the limit frequencies obtained in the experiments. The simulated combustor exhibits highly unstable eigenfrequencies between $124 < f < 153$ Hz, depending on the dispersion rate and a second eigenmode at higher frequencies

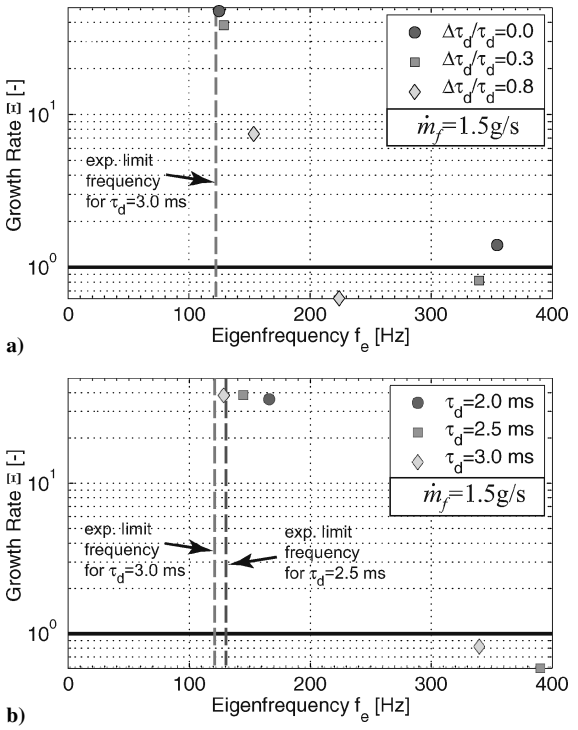

Fig. 9 Eigenfrequencies of model combustor neglecting influence of entropy waves: a) influence of different dispersion rates of droplet patterns in primary zone ($\phi = 0.55$, $\tau_d = 0.3$ ms, $\xi = 1.6$) and b) variable droplet transport times ($\phi = 0.55$, $\Delta\tau_d/\tau_d = 0.3$, $\xi = 1.6$).

above 230 Hz. The frequency of the lower unstable mode tends to increase with rising $\Delta\tau_d/\tau_d$. Compared to negligible dispersion, the growth rates have significantly decreased by 80% for $\Delta\tau_d/\tau_d = 0.8$. Stability is, however, not reached. The range of calculated eigenfrequencies in Fig. 9b agrees well with the experimental data in Fig. 2: For an estimated $\Delta\tau_d/\tau_d = 0.3$ and a droplet delay times of $\tau_d = 3$ ms corresponding to $\Delta p = 20$ mbar in the experiments, the calculated eigenfrequency is 128 vs 122 Hz measured. For decreasing τ_d, associated with rising Δp, both the eigenfrequencies and the measured limit frequencies rise. This proves the plausibility of the purely thermoacoustic origin of the self-excited instabilities in the low-frequency regime. The low-limit frequencies are not a result of the convection times of entropy waves, which were neglected in the calculation. The influence of the characteristic time scale τ_d becomes obvious in Fig. 9b. Because the geometry, the bulk flow velocities, and the temperature distribution was not changed in the combustor model, the results in Fig. 9 show that the aerodynamics of the primary zone and its droplet transport properties will impact the instability frequency. Under start-up conditions, τ_d is relatively high due to the lower airspeed and the increased timescale for accelerating the in general larger fuel droplets.[15] Despite the major influence of τ_d, the combustor instability remains to be determined by the acoustics of the entire system. With 167 Hz obtained for $\tau_d = 2$ ms and 128 Hz for $\tau_d = 3$ ms, the limit frequency rise is not inversely proportional to τ_d.

The investigation is now extended to include entropy waves, which alter the acoustic boundary conditions at the choked combustor outlet according to Eq. (24). Corresponding measurements were conducted with the venturi. Figure 10 shows the eigenfrequencies of the system for varying entropy dispersion rates $\Delta\tau_s/\tau_s$ in the dilution sector of the combustor. Compared to Fig. 9, the presence of temperature perturbations in the system leads to an increasing number of eigenfrequencies in the low-frequency regime. In the absence of entropy dispersion ($\Delta\tau_s/\tau_s = 0$), all eigenfrequencies are unstable. In Fig. 10, the vertical lines represent the experimental instability bands, shown in Fig. 3.

The lowest unstable eigenmode in Fig. 10a occurs at 85 Hz. It is related to entropy, which can be concluded from the amplitude dependence on the dispersion rate. Several higher-order entropy modes can be found at 179, 261, 332, and 383 Hz. Increasing dispersion rates of $\Delta\tau_s/\tau_s$ lead to a general shift of these eigenfrequencies toward stability and to a selective stabilization of eigenmodes. The calculated eigenfrequency for the lowest entropy mode agrees very well with the measurements in Fig. 3, where an entropy mode was detected around 85 Hz. Both in the simulation and experiment, the thermoacoustic mode at 125 Hz remains dominating. Its eigenfrequency and growth rate is altered only weakly by the effect of dispersion of the entropy waves. Under condition of low-entropy dispersion rates, the lowest entropy mode might contribute to the thermoacoustically driven self-excitation, due to the elevated growth rates observed. This also stays in agreement with the experimental findings shown in Fig. 3.

From the model equations, it can be concluded that the relative importance of the entropy and the thermoacoustic mode shifts with the operating conditions of the combustion chamber. The generated entropy wave is dominated by the temperature ratio across the flame, according to Eq. (20) and, thus, by the equivalence ratio ϕ. On the other hand, the volume increase of the flame as the driver of the thermoacoustic mode is, among others, a function of the fuel mass flow $\dot{m}_f$, according to Eq. (19). In the first phase of engine start-up, $\dot{m}_f$ tends to be low and the air fuel ratio is close to stoichiometry, which favors the entropy mode. During engine acceleration, the fuel mass flow increases, successively producing a prevailing thermoacoustic mode as seen in Fig. 3. For this reason, it is interesting to extend the investigation to the conditions of low fuel mass flows and the interaction of the modes found there. The eigenfrequencies for varying dispersion rates are shown in Fig. 10b after the fuel mass flow in the model was reduced to $\dot{m}_f = 0.5$ g/s.

Different from Fig. 10a, the entropy modes in Fig. 10b are found to dominate the instability behavior for negligible dispersion $\Delta\tau_s/\tau_s = 0$. The lowest eigenmode is obtained at 82 Hz. As before, this mode is associated with the lowest entropy mode. A corresponding mode was found experimentally at 87 Hz (Fig. 3, $\Delta p = 12$ mbar). Increasing dispersion again results in a global decrease of the growth rates and in a selective stabilization of formerly unstable modes. For high-entropy dispersion $\Delta\tau_s/\tau_s = 0.8$, almost all eigenmodes are stabilized or near stability except one, which represents the dominating instability mode for this operating point.

Figure 11 shows the instability behavior of the system at high dispersion rates of the entropy wave, $\Delta\tau_s/\tau_s = 0.8$, for a varying equivalence ratio ϕ. The equivalence ratio has been modified in the model by adapting the air mass flow while maintaining the fuel mass flow.

The overall instability behavior of the system is then influenced in a double sense: First, for low ϕ, the average bulk velocity in the combustor rises and the average residence times in the dilution zone decreases due to the higher air mass flows. Second, due to the overall leaner mixture, the temperature ratio over the flame, T_3/T_4, increases and the entropy waves produced will become weaker, following Eq. (19). As a consequence of the increase of bulk velocities in the combustor, the entropy modes in Fig. 11 are found at higher eigenfrequencies for lower ϕ. Corresponding eigenmodes for different equivalence ratios are encircled in the graph. The frequency

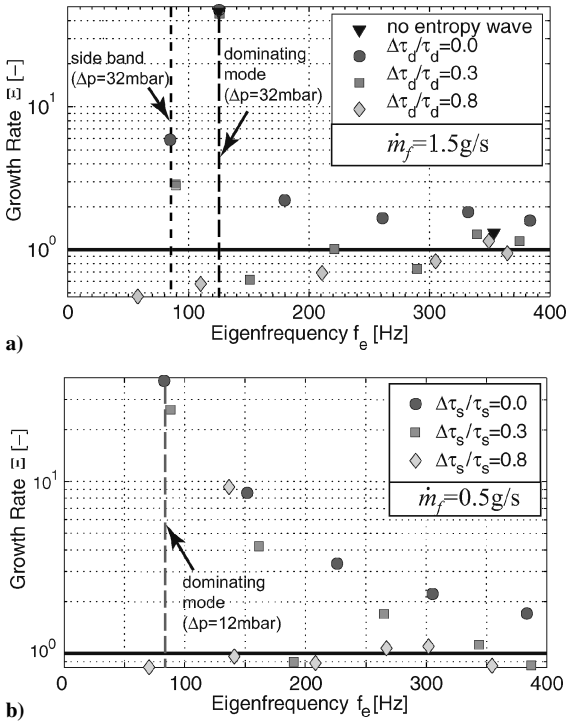

Fig. 10 Eigenfrequencies of model combustor for different dispersion rates of entropy wave $\Delta\tau_s/\tau_s$ and variable fuel mass flows $\dot{m}_f$ ($\phi = 0.55$, $\tau_d = 3$ ms, $\Delta\tau_d/\tau_d = 0.1$, $\xi = 1.6$): a) $\dot{m}_f = 1.5$ g/s and b) $\dot{m}_f = 0.5$ g/s.

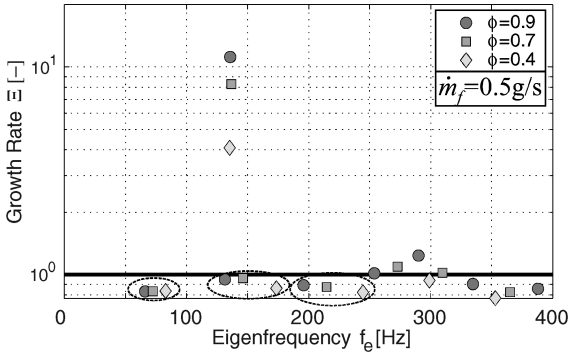

Fig. 11 Eigenfrequencies of model combustor for different equivalence ratios ϕ, varying the overall air mass flow for $\dot{m}_f = 0.5$ g/s ($\tau_d = 0.3$ ms, $\Delta\tau_d/\tau_d = 0.1$, $\Delta\tau_s/\tau_s = 0.8$, $\xi = 1.6$).

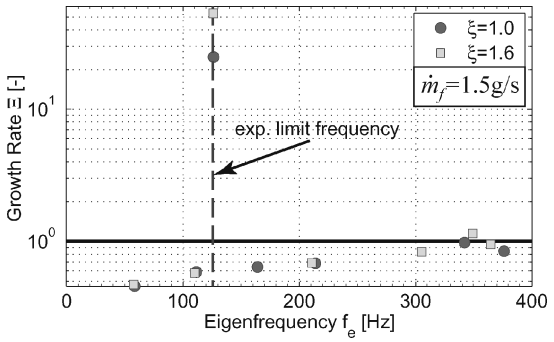

Fig. 12 Eigenfrequencies of the model combustor with venturi for different atomizer sensitivities ξ ($\phi = 0.55$, $\tau_d = 0.3$ ms, $\Delta\tau_d/\tau_d = 0.1$, $\Delta\tau_s/\tau_s = 0.8$, $\Delta\tau_s/\tau_s = 0.8$).

of the dominating unstable mode does, however, not respond to changes in τ_s, which indicates its purely thermoacoustic nature.

Another option to reduce the growth rate of the thermoacoustic mode, besides increasing the dispersion rate in the primary zone (Fig. 9a), is to reduce the injector sensitivity ξ to changing air velocities. Figure 12 shows the stability behavior of the choked combustor for varying ξ, as defined in Eq. (6). The frequency of the instability is barely affected, nor are the growth rates of the entropy modes. For a more robust injector design, for example, for $\xi = 1$, the tendency to instability decreases by 50% compared to $\xi = 1.6$ due to a lower amplitude of droplet size fluctuations, initially produced by the injector. Stability is achieved for $\xi_{\text{crit}} < 0.5$, depending on the dispersion rate and the overall applied fuel mass flow. A very similar behavior is obtained for the nonchoked configuration with flame tube.

V. Conclusions

A linear network model of a staged RQL combustor with air-blast atomization was formulated to investigate the conditions for the onset of low-frequency instabilities. The model particularly accounts for the effects of aerodynamic dispersion on overall system stability. A spray flame model was implemented, which considers the dominating influence of droplet size variations on the heat release fluctuations, as observed in prior experiments.

The dominating instability modes obtained at characteristically low-limit frequencies between 80 and 150 Hz, are of purely thermoacoustic origin and were also be obtained when neglecting the entropy waves in the model. Within the bulk oscillation mode, which is characteristic for low-frequency rumble, the obtainable limit frequencies are essentially influenced by the characteristic timescales of droplet convection in the primary combustor zone and the associated coupling of the dynamic pressure and heat release in the combustor. The presence of entropy waves were shown to impose additional eigenfrequencies on the system, which primarily respond to the average gas convection times in the dilution zone. Comparable growth rates to that of the thermoacoustic mode are only obtained for low dispersion in the dilution zone of the combustor and under conditions of low fuel mass flows, where the volume production by the flame is low. In most cases, however, the influence of entropy is weak. The parametric study has shown that the key measures for reducing rumble consists of homogenizing the droplet size variations and the droplet number densities arriving at the flame. This can be achieved by an atomizer that is less sensitive toward air velocity perturbations or that generates a highly dispersive flowfield in the primary zone.

The capability of low-order modeling to reproduce the thermoacoustic as well as entropy-driven instability behavior for spray flames has been demonstrated. The modeling of the combustor thermoacoustics was performed for rumble, exclusively considering the low-frequency range below 150 Hz. Under these conditions, the assumptions of a quasi-steady burner response and of comparably small droplet burning times were justified. To extend the model validity toward higher frequencies, the described model assumptions will have to be refined, accounting for a dynamic burner response and finite timescales of droplet evaporation and combustion.

References

[1]Keller, J. J., "Thermoacoustic Oscillations in Combustion Chambers of Gas Turbines," *AIAA Journal*, Vol. 33, No. 12, 1995, pp. 2280–2287.

[2]Marble, F. E., and Candel, S. M., "Acoustic Disturbance from Gas Non-Uniformities Convected Through a Nozzle," *Journal of Sound and Vibration*, Vol. 55, No. 2, 1977, pp. 225–243.

[3]Zhu, M., Dowling, A. P., and Bray, K. N. C., "Self-Excited Oscillations in Combustors with Spray Atomizers," *Journal of Engineering for Gas Turbines and Power*, Vol. 123, No. 4, 2001, pp. 779–786.

[4]Eckstein, J., Freitag, E., Hirsch, C., and Sattelmayer, T., "Experimental Study on the Role of Entropy Waves in Low-Frequency Oscillations for a Diffusion Burner," *Proceedings of the ASME Turbo Expo 2004*, American Society of Mechanical Engineers International, New York, 2004.

[5]Greenhalgh, D. A., Jermy, M. C., Doherty, W. G., and Hussain, M., "The Response of Fuel Injector Sprays to Acoustic Forcing," *Proceedings of the ESDA 2004, 7th Biennial ASME Conference Engineering Systems Design and Analysis*, American Society of Mechanical Engineers International, New York, 2004.

[6]Konrad, W., Brehm, N., Kameier, F., Freeman, C., and Day, I. J., "Combustion Instability Investigations on the BR710 Jet Engine," *Journal of Engineering for Gas Turbines and Power*, Vol. 120, No. 39, 1998, pp. 34–40.

[7]Sattelmayer, T., "Influence of the Combustor Aerodynamics on Combustion Instabilities from Equivalence Ratio Fluctuations," *Journal of Engineering for Gas Turbines and Power*, Vol. 125, No. 1, 2003, pp. 11–19.

[8]Sattelmayer, T., "Assessment of Methods for the Computation of the Linear Stability of Combustors," *Combustion Science and Technology*, Vol. 175, No. 3, 2003, pp. 453–476.

[9]Evesque, S., and Polifke, W., "Forced Low-Order Acoustic Modeling for Annular Combustors: Validation and Inclusion of Modal Coupling," *Proceedings of the ASME Turbo Expo 2002*, American Society of Mechanical Engineers International, New York, 2002.

[10]Lovett, J. A., and Uznanski, K. T., "Prediction of Combustion Dynamics in a Staged Premixed Combustor," *Proceedings of the ASME Turbo Expo 2002*, American Society of Mechanical Engineers International, New York, 2002.

[11]Lieuwen, T., "Modeling Premixed Combustion-Acoustic Wave Interactions: A Review," *Journal of Propulsion and Power*, Vol. 19, No. 5, 2003, pp. 765–781.

[12]Dubey, R. K., McQuay, M. Q., and Carvalho, J. A., Jr., "An Experimental and Theoretical Investigation on the Effects of Acoustics on Spray Combustion," *Twenty-Seventh Symposium (International) on Combustion*, Vol. 2, Combustion Inst., Pittsburgh, PA, 1998, pp. 2017–2023.

[13]Ghenai, C., Smith, O. I., and Karagozian, A. R., "Acoustical Excitation of Burning Fuel Droplets," AIAA Paper 2001-0328, 2001.

[14]Sujith, R. I., Waldherr, G. A., Jagoda, J. I., and Zinn, B. T., "A theoretical Investigation of the Behavior of Droplets in Axial Acoustic Fields," *Journal of Vibration and Acoustics*, Vol. 121, No. 3, 1999, pp. 286–294.

[15]Eckstein, J., Freitag, E., Hirsch, C., Sattelmayer, T., von der Bank, R., and Schilling, T., "Forced Low-Frequency Spray Characteristics of a Generic Airblast Swirl Diffusion Burner," *Journal of Engineering for Gas Turbines and Power*, Vol. 127, No. 2, 2005, pp. 301–306.

[16]Eckstein, J., "On the Mechanisms of Combustion Driven Low-Frequency Oscillations in Aero-Engines," Ph.D. Dissertation, Dept. of Mechanical Engineering, Technical Univ. of Munich, Munich, 2005, URL: http://www.td.mw.tum.de/tum-td/en/forschung/dissertationen/index_html/ [cited 20 Jan. 2005].

[17]Heilos, A., "Spektrale Analyse der thermischen Strahlungswechselwirkung in Kohlenwasserstoffflammen," *Berichte aus der Energietechnik*, Shaker Verlag, Aachen, Germany, 2002, Chap. 4.

[18]Lefebvre, A. H., *Gas Turbine Combustion*, 2nd ed., Taylor and Francis, Philadelphia, 1998, Chap. 6.

[19]Gentemann, A. M. G., Fischer, A., Evesque, S., and Polifke, W., "Acoustic Transfer Matrix Reconstruction and Analysis for Ducts with Sudden Change of Area," AIAA Paper 2003-3142, 2003.

[20]Munjal, M. L., *Acoustics of Ducts and Mufflers*, Wiley, New York, 1987.

[21]Turns, S., *An Introduction to Combustion, Concepts and Applications*, 2nd ed., McGraw–Hill, Burr Ridge, IL, 2000.

[22]Chu, B. T., "On the Generation of Pressure Waves at a Plane Flame Front," *Fourth Symposium (International) on Combustion*, Combustion Inst., Pittsburgh, PA, 1953, pp. 603–612.

[23]Polifke, W., Paschereit, C. O., and Döbbeling, K., "Constructive and Destructive Interference of Acoustic and Entropy Waves in a Premixed Combustor with a Choked Exit," *Journal of Acoustics and Vibration*, Vol. 6, No. 3, 2001, pp. 135–146.